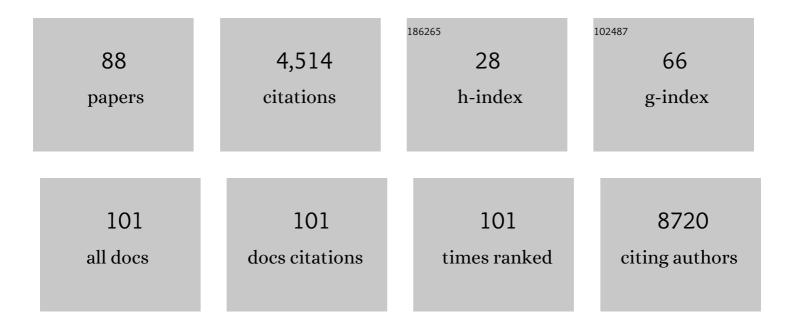
Martial Duchamp

List of Publications by Year in descending order

Source: https://exaly.com/author-pdf/8188888/publications.pdf Version: 2024-02-01



#	Article	IF	CITATIONS
1	Rational molecular passivation for high-performance perovskite light-emitting diodes. Nature Photonics, 2019, 13, 418-424.	31.4	970
2	The origin of high efficiency in low-temperature solution-processable bilayer organometal halide hybrid solar cells. Energy and Environmental Science, 2014, 7, 399-407.	30.8	965
3	Activation of surface oxygen sites on an iridium-based model catalyst for the oxygen evolution reaction. Nature Energy, 2017, 2, .	39.5	435
4	Aligned and Graded Typeâ€II Ruddlesden–Popper Perovskite Films for Efficient Solar Cells. Advanced Energy Materials, 2018, 8, 1800185.	19.5	247
5	Recrystallization-based grain boundary engineering of 316L stainless steel produced via selective laser melting. Acta Materialia, 2020, 200, 366-377.	7.9	132
6	In Situ TEM Analysis of Organic–Inorganic Metal-Halide Perovskite Solar Cells under Electrical Bias. Nano Letters, 2016, 16, 7013-7018.	9.1	115
7	Terbium-Doped VO ₂ Thin Films: Reduced Phase Transition Temperature and Largely Enhanced Luminous Transmittance. Langmuir, 2016, 32, 759-764.	3.5	112
8	Controlled Positioning of Carbon Nanotubes by Dielectrophoresis: Insights into the Solvent and Substrate Role. ACS Nano, 2010, 4, 279-284.	14.6	85
9	Time-Resolved Observations of Liquid–Liquid Phase Separation at the Nanoscale Using <i>in Situ</i> Liquid Transmission Electron Microscopy. Journal of the American Chemical Society, 2019, 141, 7202-7210.	13.7	69
10	Quantum Engineering of InAs/GaAs Quantum Dot Based Intermediate Band Solar Cells. ACS Photonics, 2017, 4, 2745-2750.	6.6	64
11	Singleâ€Crystalline Wâ€Doped VO ₂ Nanobeams with Highly Reversible Electrical and Plasmonic Responses Near Room Temperature. Advanced Materials Interfaces, 2016, 3, 1600164.	3.7	60
12	Largeâ€Area Atomic Layers of the Chargeâ€Đensityâ€Wave Conductor TiSe ₂ . Advanced Materials, 2018, 30, 1704382.	21.0	60
13	Strategies for Doped Nanocrystalline Silicon Integration in Silicon Heterojunction Solar Cells. IEEE Journal of Photovoltaics, 2016, 6, 1132-1140.	2.5	54
14	Eigenmode Tomography of Surface Charge Oscillations of Plasmonic Nanoparticles by Electron Energy Loss Spectroscopy. ACS Photonics, 2015, 2, 1628-1635.	6.6	51
15	Tuning the Plasmonic Response up: Hollow Cuboid Metal Nanostructures. ACS Photonics, 2016, 3, 770-779.	6.6	49
16	Combined model of non-conformal layer growth for accurate optical simulation of thin-film silicon solar cells. Solar Energy Materials and Solar Cells, 2013, 119, 59-66.	6.2	48
17	Single crystalline superstructured stable single domain magnetite nanoparticles. Scientific Reports, 2017, 7, 45484.	3.3	48
18	Convenient Preparation of High-Quality Specimens for Annealing Experiments in the Transmission Electron Microscope. Microscopy and Microanalysis, 2014, 20, 1638-1645.	0.4	44

#	Article	IF	CITATIONS
19	Effect of lanthanum doping on modulating the thermochromic properties of VO ₂ thin films. RSC Advances, 2016, 6, 48455-48461.	3.6	44
20	Analysis of InAs/GaAs quantum dot solar cells using Suns- V oc measurements. Solar Energy Materials and Solar Cells, 2014, 130, 241-245.	6.2	43
21	Resonances of nanoparticles with poor plasmonic metal tips. Scientific Reports, 2015, 5, 17431.	3.3	42
22	Synthesis and mechanical properties of carbon nanotubes produced by the water assisted CVD process. Physica Status Solidi (B): Basic Research, 2009, 246, 2457-2460.	1.5	38
23	Atomic-scale quantification of charge densities in two-dimensional materials. Physical Review B, 2018, 98, .	3.2	36
24	A diecast mineralization process forms the tough mantis shrimp dactyl club. Proceedings of the National Academy of Sciences of the United States of America, 2019, 116, 8685-8692.	7.1	33
25	Effect of Zinc Incorporation on the Performance of Red Light Emitting InP Core Nanocrystals. Inorganic Chemistry, 2016, 55, 8381-8386.	4.0	31
26	Enhancing the optoelectronic properties of amorphous zinc tin oxide by subgap defect passivation: A theoretical and experimental demonstration. Physical Review B, 2017, 95, .	3.2	31
27	Uniformly dispersed deposition of colloidal nanoparticles and nanowires by boiling. Applied Physics Letters, 2007, 91, 173112.	3.3	30
28	New progress in the fabrication of n–i–p micromorph solar cells for opaque substrates. Solar Energy Materials and Solar Cells, 2013, 114, 147-155.	6.2	29
29	STEM–EELS analysis reveals stable high-density He in nanopores of amorphous silicon coatings deposited by magnetron sputtering. Nanotechnology, 2015, 26, 075703.	2.6	29
30	Mechanical and electronic properties of vanadium oxide nanotubes. Journal of Applied Physics, 2009, 105, .	2.5	26
31	Understanding the Role of Single Molecular ZnS Precursors in the Synthesis of In(Zn)P/ZnS Nanocrystals. ACS Applied Materials & Interfaces, 2014, 6, 18233-18242.	8.0	26
32	Graphoepitaxy of Highâ€Quality GaN Layers on Graphene/6H–SiC. Advanced Materials Interfaces, 2015, 2, 1400230.	3.7	23
33	Quantitative measurement of mean inner potential and specimen thickness from high-resolution off-axis electron holograms of ultra-thin layered WSe2. Ultramicroscopy, 2017, 178, 38-47.	1.9	23
34	Effect of TaN intermediate layer on the back contact reaction of sputter-deposited Cu poor Cu2ZnSnS4 and Mo. Applied Surface Science, 2019, 471, 277-288.	6.1	21
35	Compositional study of defects in microcrystalline silicon solar cells using spectral decomposition in the scanning transmission electron microscope. Applied Physics Letters, 2013, 102, .	3.3	20
36	Giant resistive switching in mixed phase BiFeO ₃ <i>via</i> phase population control. Nanoscale, 2018, 10, 17629-17637.	5.6	18

#	Article	IF	CITATIONS
37	Generation of electron vortices using nonexact electric fields. Physical Review Research, 2020, 2, .	3.6	18
38	On stoichiometry and intermixing at the spinel/perovskite interface in CoFe2O4/BaTiO3 thin films. Nanoscale, 2015, 7, 218-224.	5.6	17
39	Production of high quality carbon nanotubes for less than \$1 per gram. Physica Status Solidi C: Current Topics in Solid State Physics, 2010, 7, 1236-1240.	0.8	16
40	Reinforcing multiwall carbon nanotubes by electron beam irradiation. Journal of Applied Physics, 2010, 108, 084314.	2.5	16
41	<i>In situ</i> transmission electron microscopy of resistive switching in thin silicon oxide layers. Resolution and Discovery, 2016, 1, 27-33.	0.4	16
42	Generation of electron vortex beams using line charges via the electrostatic Aharonov-Bohm effect. Ultramicroscopy, 2017, 181, 191-196.	1.9	16
43	Mechanical response of CH3NH3PbI3 nanowires. Applied Physics Letters, 2018, 112, .	3.3	15
44	Carrier scattering mechanisms limiting mobility in hydrogen-doped indium oxide. Journal of Applied Physics, 2018, 123, .	2.5	15
45	Enhanced Spin Hall Effect in Sâ€Implanted Pt. Advanced Quantum Technologies, 2021, 4, .	3.9	15
46	Vapor transport growth of MoS2 nucleated on SiO2 patterns and graphene flakes. Nano Research, 2016, 9, 3504-3514.	10.4	14
47	Challenges and Applications to <i>Operando</i> and <i>In Situ</i> TEM Imaging and Spectroscopic Capabilities in a Cryogenic Temperature Range. Accounts of Chemical Research, 2021, 54, 3125-3135.	15.6	13
48	Atomic resolution imaging and spectroscopy of barium atoms and functional groups on graphene oxide. Ultramicroscopy, 2014, 145, 66-73.	1.9	12
49	Quenching of TiO2 photo catalysis by silver nanoparticles. Journal of Photochemistry and Photobiology A: Chemistry, 2012, 230, 10-14.	3.9	11
50	Effect of post-growth annealing on secondary phase formation in low-temperature-grown Mn-doped GaAs. Journal Physics D: Applied Physics, 2013, 46, 145309.	2.8	9
51	Direct observation of doping incorporation pathways in self-catalytic GaMnAs nanowires. Journal of Applied Physics, 2015, 118, .	2.5	9
52	Intrinsic electronic properties of high-quality wurtzite InN. Physical Review B, 2016, 94, .	3.2	8
53	Zig-zag Self-assembly of Magnetic Octahedral Fe3O4 Nanocrystals using in situ Liquid Transmission Electron Microscopy. Microscopy and Microanalysis, 2016, 22, 36-37.	0.4	8
54	New experiments with a double crystal electron interferometer. EPJ Applied Physics, 2017, 78, 10701.	0.7	8

#	Article	IF	CITATIONS
55	Magnetoimpedance of Epitaxial Y ₃ Fe ₅ O ₁₂ (001) Thin Film in Low-Frequency Regime. ACS Applied Materials & Interfaces, 2020, 12, 41802-41809.	8.0	8
56	Atomic resolution enabled STEM imaging of nanocrystals at cryogenic temperature. JPhys Materials, 2020, 3, 034006.	4.2	8
57	Electron energy-loss spectroscopy of boron-doped layers in amorphous thin film silicon solar cells. Journal of Applied Physics, 2013, 113, .	2.5	7
58	STEM electron beam-induced current measurements of organic-inorganic perovskite solar cells. Ultramicroscopy, 2020, 217, 113047.	1.9	7
59	Defects in paramagnetic Co-doped ZnO films studied by transmission electron microscopy. Journal of Applied Physics, 2013, 114, .	2.5	6
60	Microstructural characterization of Cr-doped (Bi,Sb) ₂ Te ₃ thin films. CrystEngComm, 2017, 19, 3633-3639.	2.6	6
61	Multi-modal and multi-scale non-local means method to analyze spectroscopic datasets. Ultramicroscopy, 2020, 209, 112877.	1.9	6
62	Facet controlled anisotropic magnons in Y3Fe5O12 thin films. Applied Physics Letters, 2021, 119, .	3.3	6
63	Recovery Mechanisms in Aged Kesterite Solar Cells. ACS Applied Energy Materials, 2022, 5, 5404-5414.	5.1	6
64	EELS measurements of boron concentration profiles in p-a-Si and nip a-Si solar cells. Journal of Non-Crystalline Solids, 2012, 358, 2179-2182.	3.1	5
65	GaN heterostructures with diamond and graphene. Semiconductor Science and Technology, 2015, 30, 114001.	2.0	5
66	Fine electron biprism on a Si-on-insulator chip for off-axis electron holography. Ultramicroscopy, 2018, 185, 81-89.	1.9	5
67	Real-Time Electron Nanoscopy of Photovoltaic Absorber Formation from Kesterite Nanoparticles. ACS Applied Energy Materials, 2020, 3, 122-128.	5.1	5
68	Strain and compositional fluctuations in Al0.811n0.19N/GaN heterostructures. Applied Physics Letters, 2016, 109, 132102.	3.3	4
69	Operando Direct Observation of Filament Formation in Resistive Switching Devices Enabled by a Topological Transformation Molecule. Nano Letters, 2021, 21, 9262-9269.	9.1	4
70	Design and fabrication of InAs/GaAs QD based intermediate band solar cells by quantum engineering. , 2018, , .		3
71	Mapping atomic electric fields and charge densities by four-dimensional STEM. Acta Crystallographica Section A: Foundations and Advances, 2017, 73, C119-C119.	0.1	2
72	Exploring two dimensional Co0.33In2.67S2.29Se1.71 as alloy type negative electrode for Li-ion battery with olivine LiFePO4 cathode. Materials Today Energy, 2018, 9, 19-26.	4.7	2

#	Article	IF	CITATIONS
73	Quantum engineering InAs/GaAs single-junction concentrator solar cells (Conference Presentation). , 2018, , .		2
74	Mapping boron in silicon solar cells using electron energy-loss spectroscopy. Journal of Physics: Conference Series, 2011, 326, 012052.	0.4	1
75	Conventional and 360 degree electron tomography of a micro-crystalline silicon solar cell. Journal of Physics: Conference Series, 2011, 326, 012057.	0.4	1
76	Measurement of Atomic Electric Fields by Scanning Transmission Electron Microscopy (STEM) Employing Ultrafast Detectors. Microscopy and Microanalysis, 2016, 22, 484-485.	0.4	1
77	Denoising Electron-energy Loss Data Using Non-local Means Filters. Microscopy and Microanalysis, 2017, 23, 106-107.	0.4	1
78	Reflectance Improvement by Thermal Annealing of Sputtered Ag/ZnO Back Reflectors in a-Si:H Thin Film Silicon Solar Cells. Materials Research Society Symposia Proceedings, 2011, 1321, 63.	0.1	0
79	Silicon-Light: a European project aiming at high efficiency thin film silicon solar cells on foil. EPJ Photovoltaics, 2014, 5, 55203.	1.6	0
80	Three-dimensional Surface Charge Reconstructions of Surface Plasmon Modes of Silver Right Bipyramids. Microscopy and Microanalysis, 2015, 21, 2225-2226.	0.4	0
81	Electric and Magnetic Field Mapping With the pnCCD (S)TEM Camera. Microscopy and Microanalysis, 2016, 22, 256-257.	0.4	0
82	Hollow metal nanostructures for enhanced plasmonics (Conference Presentation). , 2016, , .		0
83	High Temperature Stability of Amorphous Zn-Sn-O Transparent Conductive Oxides Investigated by In Situ TEM and X-ray Diffraction. Microscopy and Microanalysis, 2016, 22, 1582-1583.	0.4	0
84	What Limits Mobility in Hydrogenated Indium Oxide?. , 2018, , .		0
85	Investigation of the Oxidation Reaction of LiFePO4 Cathode Material using Environmental TEM. Microscopy and Microanalysis, 2019, 25, 1858-1859.	0.4	Ο
86	Elastic distortion determining conduction in BiFeO ₃ phase boundaries. RSC Advances, 2020, 10, 27954-27960.	3.6	0
87	Operando and in situ in a TEM imaging in a cryogenic temperature range. Microscopy and Microanalysis, 2021, 27, 386-387.	0.4	0
88	Innovative fabrication of low-cost kesterite solar cells for distributed energy applications. , 2020, , .		0